Chemical Engineering Journal 425 (2021) 131508

Contents lists available at ScienceDirect

Chemical Engineering Journal

journal homepage: www.elsevier.com/locate/cej

On-line control of particle morphology of waterborne dispersed polymers using master trajectories

Nicholas Ballard [a,b], Wolfgang Gerlinger [c], José M. Asua [a,*]

[a] POLYMAT, Kimika Aplikatu Saila, Kimika Fakultatea, University of the Basque Country UPV/EHU, Avda Tolosa 72, Donostia-San Sebastián 20018, Spain
[b] Ikerbasque, Basque Foundation for Science, Bilbao 48013, Spain
[c] BASF SE, Ludwigshafen, Germany

ARTICLE INFO

Keywords:
Particle morphology
Online control
Emulsion polymers
Process optimization

ABSTRACT

On-line control of the morphology of waterborne composite latex particles is an unsolved issue because of the lack of techniques for on-line monitoring of particle structure. As an alternative to online monitoring, soft sensors based on detailed mathematical models for the development of particle morphology can be used but they require knowledge of a large number of system-specific parameters and, therefore, they are not suitable for a market characterized by large portfolios of products. This work presents a new method to achieve control over final particle morphology by using master trajectories obtained from a given reference process as set points. The master trajectories are derived from the understanding of the fundamental phase separation and phase migration processes occurring during the development of the particle morphology, and can be estimated during the process from available on-line measurements (overall and instantaneous monomer conversion, and reactor temperature). The approach opens the way to on-line control of the particle morphology and can also be used for process optimization.

1. Introduction

Multiphase latex particles are an important class of polymer dispersions that are widely used in coatings [1–6] and adhesives [7–10], as well as in a number of niche markets [11–13]. In these systems, the particle morphology is often crucial in determining the final properties of the material and, therefore, controlling the particle morphology during the production of the latex is of great importance. In general, particle morphology is governed by the balance between minimization of the total interfacial energy, which drives the system towards the equilibrium morphology, and the resistance to movement caused by the viscosity of the particle. When this resistance is smaller than the driving force, the equilibrium morphology is reached. For two-phase systems there is a limited number of equilibrium morphologies (core-shell, hemispherical and inverted core-shell) that are reasonably well understood [14–16]. However, in many cases out of equilibrium morphologies are desired, which requires careful control over the polymerization process [17–21].

Despite its technological importance, on-line control of the morphology of waterborne composite particles remains an unsolved issue, largely due to the lack of practical techniques for on-line monitoring of the particle morphology. Open-loop control works well in the absence of disturbances [22], but emulsion polymerization often suffers from poor run-to-run reproducibility [23] making it difficult to practically implement such strategies. Rajabalinia et al. [24] recently demonstrated experimentally that good control of the particle morphology in the presence of disturbances can be achieved by controlling both instantaneous and overall conversions and matching them to a reference process. The rationale behind this work was that particle morphology can be controlled if the reaction conditions within the particles are reproduced. Whereas this strategy clearly works for the disturbance studied (a sudden decrease of the polymerization rate caused by a shot of inhibitor), it will likely fail in the case of a disturbance caused by a failure in the reactor cooling system (leading to uncontrolled increases in instantaneous conversion) or when the process is carried out in a reactor with a different heat removal capacity (requiring changes in overall process time).

In the absence of direct on-line measurements of the particle morphology, on-line control has to rely on the use of soft sensors. A potential way of achieving this is through use of a mathematical model able to calculate the evolution of the particle morphology from kinetic data, in particular from on-line measurements of monomer conversions

* Corresponding author.
E-mail address: jm.asua@ehu.eus (J.M. Asua).

https://doi.org/10.1016/j.cej.2021.131508
Received 4 June 2021; Received in revised form 21 July 2021; Accepted 24 July 2021
Available online 9 August 2021

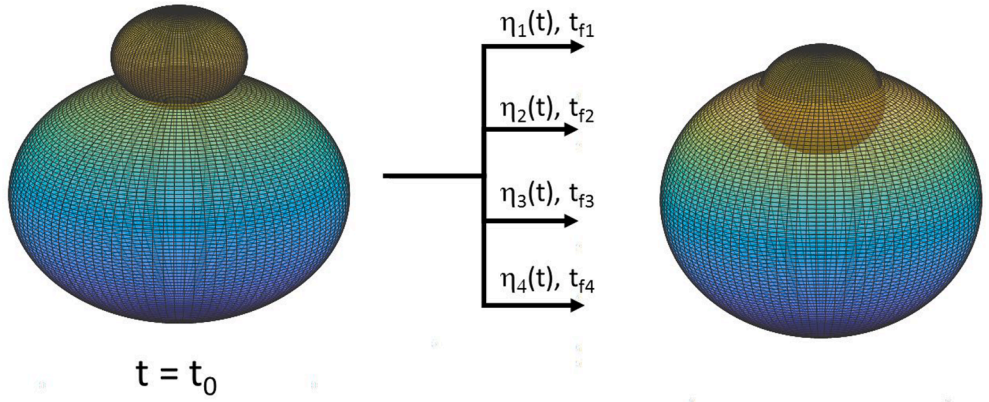

Fig. 1. Reaction trajectories and evolution of the particle morphology.

and reactor temperature. A mathematical model for the evolution of the particle morphology of waterborne dispersed polymers has been recently developed [25] and it describes well the evolution of the particle morphology for polymer-polymer [26] and polymer-inorganic [27] systems. The model has also been used for process optimization [28]. While the use of this model as a soft sensor is promising, the applicability of this approach is limited by the accuracy of the model, as has been demonstrated *in silico* [29]. Furthermore, there are practical challenges associated with this approach as this implies the development of a model for each system, which can be acceptable for some large tonnage products, but is not desirable in a market that is characterized by large portfolios of products. Therefore, there is a need for a reliable soft sensor that uses only available on-line measurements and does not require a precise mathematical model for the particle morphology dynamics.

This work is an attempt to develop such a reliable soft sensor that will lead to the control of the particle morphology of composite waterborne polymer dispersions using only on-line measurements of monomer conversions and reactor temperature. At the core of this idea is the concept of a master trajectory that defines the development of particle morphology. Therefore, the master curves can be used as set points for on-line control of the particle morphology subject to given constraints such as reaction time or reactor temperature. The paper is organized as

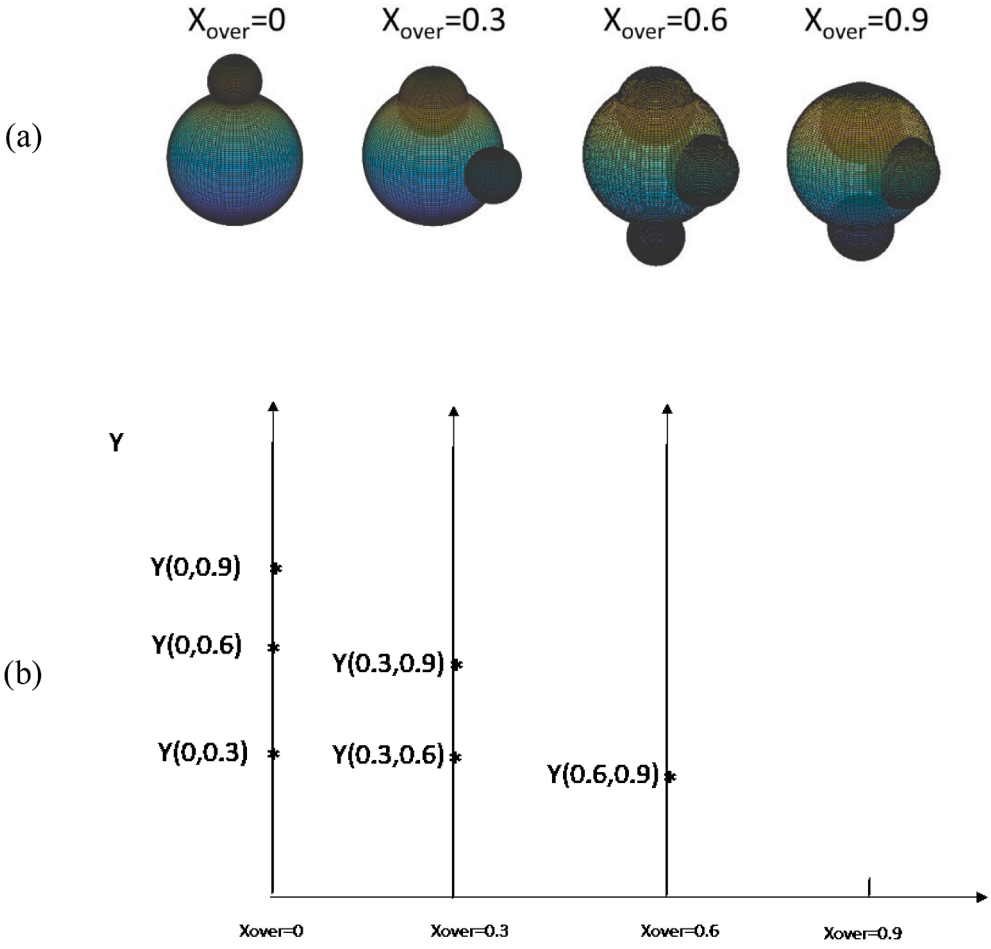

Fig. 2. Relative movement of clusters formed at different moments in the process.

follows. In the next section, we will demonstrate the underlying concepts that allow for the construction of the master curve describing the evolution of particle morphology and how it may be used. In the subsequent sections we demonstrate the validity of the concept using both *in silico* and experimental data. Finally, the opportunities that the proposed strategy can provide in terms of process optimization are discussed.

2. Master curves for the development of particle morphology

2.1. Forces involved in the development of particle morphology

Let us consider a seeded semicontinuous emulsion polymerization process, which is the most common way of producing commercial polymer-polymer composite waterborne dispersions. This process is carried out under conditions in which both secondary nucleation and particle coagulation are avoided, namely with a constant number of particles in the system. The seed is formed by Polymer 1. During the semibatch process, clusters of the newly generated polymer (Polymer 2) are formed by phase separation due to polymer–polymer incompatibility. Phase separation occurs when the concentration of Polymer 2 in the monomer-swollen seed exceeds the solubility limit. Similar to what occurs in the formation of particles by homogeneous nucleation, the formation of the new clusters is strongly affected by the existence of previous clusters as polymer chains and the newly formed clusters may be captured by the existing clusters. Therefore, the rate of cluster formation is largely determined by the number, size and position of the previously formed clusters. The position in the particle where the clusters are formed depends on the type of initiator used (water-soluble vs. oil-soluble) and no significant changes are expected during the controlled polymerization if particles of the same size and the same initiator are used.

The evolution of the particle morphology occurs due to the movement of these clusters over time. The movement depends on both the driving forces and the drag forces. The driving forces for this movement are the interfacial tensions and van der Waals interactions, both of which are not expected to vary significantly from run to run if the same polymers and surfactants are used (this restriction will be released later). The drag forces are related to the viscosity of the interior of the particle (η). The interior of the particle is the monomer swollen seed polymer (Polymer 1) and will be referred to as the particle matrix. Under these circumstances, the movement of the clusters can be described as [19]:

$$\frac{dY}{dt} = \frac{k_1}{\eta} \tag{1}$$

where Y is the distance, t the time, k_1 is a parameter that includes the driving force, and η the viscosity of the particle matrix.

Therefore, the distance that a cluster can travel from the moment in which is formed (t_0) until the end of the process (t_f) is

$$Y_{final} = \int_{t_0}^{t_f} \frac{k_1}{\eta(t)} dt \tag{2}$$

Fig. 1 helps to understand the implications of Eq. (2) on particle morphology. Let us consider that at time t_0, there is a cluster of Polymer 2 at the surface of the polymer particle and that Polymer 2 is more hydrophobic than Polymer 1. Under these circumstances, the cluster will migrate towards the center [30,31]. Eq. (2) predicts that there are an infinite number of trajectories characterized by different η(t) and t_f that will bring the cluster to the position depicted in the right figure, namely to the same penetration. The movement of the cluster depends on the driving force, the viscosity of the polymer matrix, the position of the cluster in the particle, and the characteristics of the cluster (e.g., cluster size). All these properties change over time.

Let us now consider the case of clusters produced at different moments in the process that are defined by the overall conversion ($X_{over}(t)$),

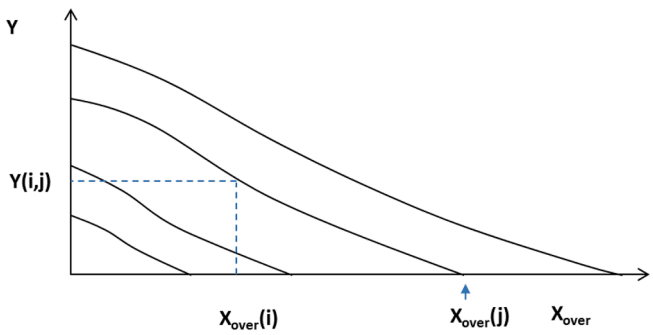

Fig. 3. Cluster trajectories.

which is given by

$$X_{over}(t) = \frac{Pol_2(t)}{M_{2tot}} \tag{3}$$

where $Pol_2(t)$ is the mass of second stage polymer formed up to time t, and M_{2tot} is the total amount of second stage monomer(s) to be fed into the system.

Fig. 2 illustrates the case of clusters formed at different overall conversions (X_{over} = 0, 0.3 and 0.6). The first cluster was formed at X_{over} = 0. When the second cluster was formed at X_{over} = 0.3, the first cluster has penetrated a certain distance (Y(0, 0.3) in Fig. 2b). The third cluster was formed at X_{over} = 0.6, and by then, the clusters formed previously had penetrated distances Y(0, 0.6) and Y(0.3, 0.6). It is worth pointing out that, as illustrated in Fig. 2b, the distance covered by the first cluster in the time interval between conversions 0.3 and 0.6, will most likely be different from the distance covered by the second cluster. The reason can be explained as follows. The distance covered by a cluster formed at X_{over} = 0 during this period is

$$Y_{0.3\to0.6}^{0} = k_0 \int_{t0.3}^{t0.6} \frac{1}{\eta(t)} dt \tag{4}$$

This distance is determined by the characteristics of the cluster (k_0), the environment in which the cluster moves (η) and the times at the two conversions. It is worth pointing out that k_0 is an average characteristic as the cluster changes over time (it grows in size).

Similarly, for the cluster formed at X_{over} = 0.3, the distance covered between conversions 0.3 and 0.6 is

$$Y_{0.3\to0.6}^{0.3} = k_{0.3} \int_{t0.3}^{t0.6} \frac{1}{\eta(t)} dt \tag{5}$$

where $k_{0.3}$ characterizes this cluster (different from k_0). As k_0 and $k_{0.3}$ are different, the distance covered by the clusters is different. Between X_{over} = 0.6 and X_{over} = 0.9, the three clusters moved towards the interior of the particle.

2.2. Master curves

In the example above, clusters formed at specific moments in the process were considered, but as clusters are formed continuously, rather than at individual points, the movement of the clusters formed up to a certain moment will be described by a continuous line. The line describes the trajectories of all clusters previously formed. Fig. 3 illustrates the trajectories for various moments in the polymerization that are defined by the overall conversion at which the curve intercepts the X axis. Thus, a cluster formed when the overall conversion was X_{over}(i) will be at Y(i,j) when the overall conversion is X_{over}(j).

We hypothesized that any polymerization for which the clusters follow the trajectories in Fig. 3 will yield the same particle morphology. Therefore, if the hypothesis is correct, these trajectories could be used for controlling the particle morphology.

At first sight, the hypothesis might look simplistic as cluster nucleation and cluster coalescence also play a role in the development of the particle morphology. Nevertheless, in what follows we will demonstrate how powerful the concept of the cluster trajectories is. Let us consider that a given particle morphology has been obtained in a seeded semi-continuous emulsion polymerization process and that this product gives good application properties. The process used to obtain this morphology will be called the reference process. Therefore, it is of interest to develop a control scheme that ensures the robust production of this morphology. It is worth pointing out that the number of particles in the latex ($N_p = 6w_{pol}/\pi\rho_{pol}d_p^3$ where w_{pol} is the weight of polymer, ρ_{pol} is the density of the polymer and d_p is the particle diameter) is very high, giving for example 5.5×10^{17} particles L^{-1} for a 50 wt% solids latex with an average particle diameter of 120 nm. For the out-of-equilibrium morphologies that are explored here, each particle has a distinct morphology and therefore, in this context of this work, particle morphology really means a distribution of morphologies.

The sought morphology is the result of the creation of clusters at certain moments of the process (defined by the overall conversion) and their subsequent migration and coalescence. Therefore, control will be achieved if at any overall conversion, a) the rate of creation of clusters is similar to that in the reference process at the same overall conversion, and b) for the rest of the process, the resistance to the movement of these clusters through the matrix is also similar to that of the reference process. Cluster coalescence depends on the number of clusters and their mobility. Therefore, for the same cluster nucleation and migration, cluster coalescence is expected to be similar. This point is discussed in the results section.

There is no way to measure the rate of cluster formation, but for control purposes the only necessary condition is that this rate should be the same as in the reference process. A way to achieve this is to make sure that, at any overall conversion, the clusters are formed in an environment (particle morphology) that is close to that of the reference process. In other words, that at any overall conversion, the polymer particles in the controlled process and in the reference process have similar morphology. Both the reference and controlled processes have the same initial environment: the monomer swollen seed. Therefore, the initial rate of cluster formation is expected to be similar. Let us consider the contribution of these initial clusters to the particle morphology at an overall conversion X_{over1}. Both in the reference and in the controlled process, the clusters have grown due to the increase in overall conversion. Therefore, they will be similar in size. On the other hand, they have moved the following distances:

$$Y_{ref} = k_0 \int_0^{t_{ref}(X_{over1})} \frac{1}{\eta_{ref}(t)} dt \tag{6}$$

$$Y_{control} = k_0 \int_0^{t_{control}(X_{over1})} \frac{1}{\eta_{control}(t)} dt \tag{7}$$

Notice that as the clusters are similar they will have the same k_0, but viscosities and process times needed to reach X_{over1} may be different. Therefore, in order to move the same distance,

$$\int_0^{t_{ref}(X_{over1})} \frac{1}{\eta_{ref}(t)} dt = \int_0^{t_{control}(X_{over1})} \frac{1}{\eta_{control}(t)} dt \tag{8}$$

If Eq. (8) is fulfilled at X_{over1}, the contribution of the clusters formed at the beginning of the process to the particle morphology will be the same in both the reference and the controlled process. The beauty of Eq. (8) is that the proportionality constant (k_0) has disappeared. Applying the same reasoning to the clusters formed at overall conversions smaller than X_{over1}, the particle morphology achieved in the controlled and reference processes at X_{over1} will be same if

$$\int_{t_{ref}(X_{over})}^{t_{ref}(X_{over1})} \frac{1}{\eta_{ref}(t)} dt = \int_{t_{control}(X_{over})}^{t_{control}(X_{over1})} \frac{1}{\eta_{control}(t)} dt \quad \text{for} \quad 0 \le X_{over} \le X_{over1} \tag{9}$$

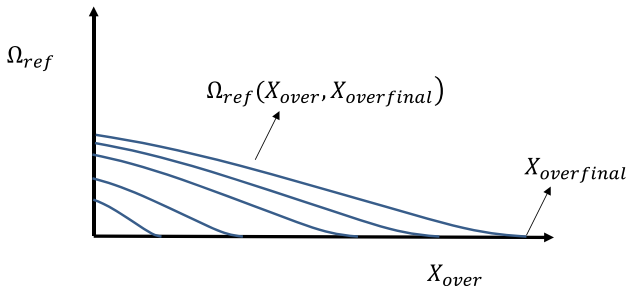

Fig. 4. Master curves at different overall conversions for the reference process.

For convenience a new magnitude is defined as

$$\Omega_{ref}(X_{over}, X_{over1}) = \int_{t_{ref}(X_{over})}^{t_{ref}(X_{overf1})} \frac{1}{\eta_{ref}(t)} dt \tag{10}$$

$\Omega_{ref}(X_{over}, X_{over1})$ is represented in Fig. 4 and is related to the resistances that the trajectories of the clusters formed up to X_{over1} should overcome. Two processes that fulfill the same line at X_{over1} will have the same particle morphology because in both processes the rate of cluster generation at a given overall conversion is the same and the clusters have overcome the same resistances to movement.

Eq. (9) and Eq. (10) can be extended to all conversions including the final conversion as follows

$$\int_{t_{ref}(X_{over})}^{t_{ref}(X_{over\ final})} \frac{1}{\eta_{ref}(t)} dt = \int_{t_{control}(X_{over})}^{t_{control}(X_{over\ final})} \frac{1}{\eta_{control}(t)} dt \quad for \quad 0 \le X_{over} \le X_{over\ final} \tag{11}$$

$$\Omega_{ref}(X_{over}, X_{over\ final}) = \int_{t_{ref}(X_{over})}^{t_{ref}(X_{over\ final})} \frac{1}{\eta_{ref}(t)} dt \quad for \quad 0 \le X_{over} \le X_{over\ final} \tag{12}$$

where $\Omega_{ref}(X_{over}, X_{overfinal})$ represents the locus that determines the resistances that all clusters formed during the whole process have overcome. Two processes that have the same $\Omega(X_{over}, X_{overfinal})$ will have the same particle morphology, namely $\Omega_{ref}(X_{over}, X_{overfinal})$ is a master curve. The set of curves represented in Fig. 4 are master curves for different overall conversions.

These master curves can be used as set points for the control of the particle morphology as they can be determined from available on-line measurements of temperature and instantaneous and overall conversions by using a rheological model to calculate the viscosity of the matrix. The viscosity of the particle depends on the polymer content (ϕ_{pol}), reaction temperature (T) and glass transition temperature of the seed polymer (T_{gpol}). A commonly used equation is [32]

$$\eta(t) = A\phi_{pol}^5(t)\exp\left(B\left(\frac{T_{geffect}(t)}{T(t)} - C\right)\right) \tag{13}$$

where A, B and C are parameters that can be estimated from rheological measurements, ϕ_{pol} is the polymer volume fraction and $T_{geffect}$ is the effective T_g of the monomer swollen Polymer 1 given by [33]

$$T_{geffect} = \frac{T_{gpol} + (KT_{gM} - T_{gpol})\phi_M}{1 + (K-1)\phi_M} \tag{14}$$

where T_{gM} is the glass transition temperature of the monomer, ϕ_M the volume fraction of the monomer and K a constant that typically varies from 1 to 3. Based on previous studies of the effect of solvents on the glass transition temperature of concentrated pMMA-solvent sytems[32], $K = 2$ was used in this work. It is worth pointing out that even in isothermal processes, the exponential term in Eq. (13) is not constant as it depends on the concentration of monomer in the particles, namely on

Table 1
Formulation used in the reference seeded emulsion polymerization.

Seed	35 wt% solids content, MMA/BA (75/25 wt/wt), Tg = 60 °C, dp = 220 nm
Monomer feed	BA/S (33/67 wt/wt), seed/monomer fed = 1/1 wt/wt;
Initiator system	TBHP (initial charge)/AsAc (fed) (1/1 mol/mol), TBHP/monomer fed = 1/200 wt/wt;
Temperature	80 °C
Process time	Feeding time = 10000 s; total time = 13000 s
Final solids content	50 wt%

X_{inst}. In order to accurately determine both ϕ_{pol} and $T_{geffect}$ the partitioning of the monomer between the different phases of the particle and the aqueous phase should be calculated using the available methods [34]. Nevertheless, in this work an approximation is used taking into account that the monomer typically partitions evenly among the different phases of the particle and that for solids contents above 30%, which is typical of most commercial processes, almost all the monomer is in the polymer particles [35]. Under these circumstances, the volume fraction of polymer in the matrix of the particle is given by

$$\phi_{pol} = \frac{\frac{Pol_1}{\rho_1} + \frac{Pol_2}{\rho_2}}{\frac{M_2(t) - Pol_2}{\rho_{mon2}} + \frac{Pol_1}{\rho_1} + \frac{Pol_2}{\rho_2}} \tag{15}$$

where Pol_1 is the mass of the seed polymer, Pol_2 is that of the newly formed polymer, $M_2(t)$ is the mass of the second stage monomer(s) fed until time t, and ρ_i is the density of compound i. It is worth pointing out that Pol_2 is related to the instantaneous conversion of monomer 2 as

$$X_{inst2} = \frac{Pol_2}{M_2(t)} \tag{16}$$

However, for convenience, the instantaneous conversion is defined as

$$X_{inst} = \frac{Pol_1 + Pol_2}{M_2(t) + Pol_1} \tag{17}$$

Note that with this definition and the assumptions leading to Eq. (15), X_{inst} is very close to ϕ_{pol}.

The existence of the master curves would be a breakthrough in the long time standing, and so far unsolved, problem of the on-line control of particle morphology. These master curves can be calculated from the reference experiment using only the time evolutions of the reactor temperature (T(t)) and instantaneous ($X_{inst}(t)$) and overall ($X_{over}(t)$) conversions. Subsequently the master curve can be used as set point in a controlled process, because $\Omega_{control}(X_{over}, X_{over1})$ can be calculated at any moment and compared with the set point. In the next section we test the validity of this concept by comparison of the particle morphology of processes that achieve the same trajectory on the master curve but with different evolutions of T(t), $X_{inst}(t)$ and $X_{over}(t)$.

3. Demonstration that $\Omega_{ref}(X_{over}, X_{overfinal})$ is a master curve

3.1. *In silico* demonstration that $\Omega_{ref}(X_{over}, X_{overfinal})$ is a master curve

For the *in silico* demonstration, the mathematical model recently developed for the dynamics of particle morphology was used to simulate the process [25]. The model, which is summarized in the Supporting Information, provides the time evolution of the monomer conversions as well as the particle morphology characterized by the distributions of clusters in equilibrium and non-equilibrium positions. In the example considered, the monomers used in the formulation (Table 1) yield a polymer that is more hydrophobic than the seed polymer, therefore, the equilibrium position is the center of the particle [30,31]. Consequently, there will be a single equilibrium cluster per particle. The use of water-soluble initiators leads to a radical concentration profile within the polymer particle due to diffusion limitations of radicals that enter at the particle surface. The model accounts for this by considering that in terms of radical concentration, the particle can be divided into two regions: an outer shell (region 1) where the concentration of radicals is high and an inner region (region 2) where the concentration of radicals is low. It is worth pointing out that this inner region includes the equilibrium cluster. Although methods to estimate the size of these regions and the ratio of concentration of radicals have been developed[26], in these simulations it was considered that during the whole polymerization, the volume fraction of region 1 in the particle was 0.48 and that the ratio between the radical concentrations in regions 1 and 2 was 1000. These values are based on estimates from previous work using similar systems [26].

First, a reference semicontinuous seeded emulsion polymerization was simulated at constant temperature (80 °C) and constant feeding rates of the monomers using the formulation in Table 1. Fig. 5 presents the evolutions of the instantaneous and overall conversions. At the beginning of the experiment, the instantaneous conversion that initially is $X_{inst} = 1$ (seed polymer) decreases due to the addition of monomer and subsequently reaches a near steady state with a constant rate of polymerization and an instantaneous conversion of around 0.95 during the monomer feeding stage. After monomer feeding is stopped at 10000 s, the instantaneous conversion increases as the residual monomer in the reactor is consumed.

Fig. 6 shows the final particle morphology characterized by the cluster size distributions in the different locations within the particle. Note that this figure shows the normalized weight distribution obtained by multiplying the number distributions by the cluster size (x). These distributions show the size of the non-equilibrium clusters in the outer region ($m_1(x)$) and in the inner region ($m_2(x)$), as well as that of the equilibrium clusters (n(x)). It is important to note that these distribution

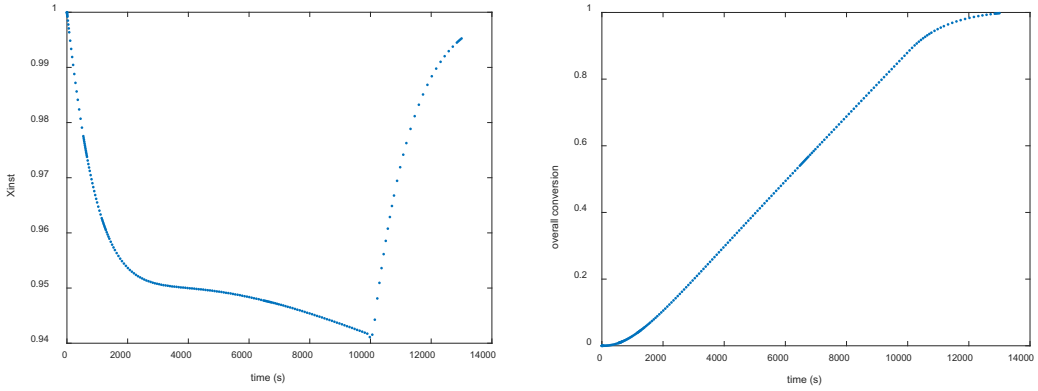

Fig. 5. Time evolution of the instantaneous and overall conversions in the reference semicontinuous seeded emulsion polymerization.

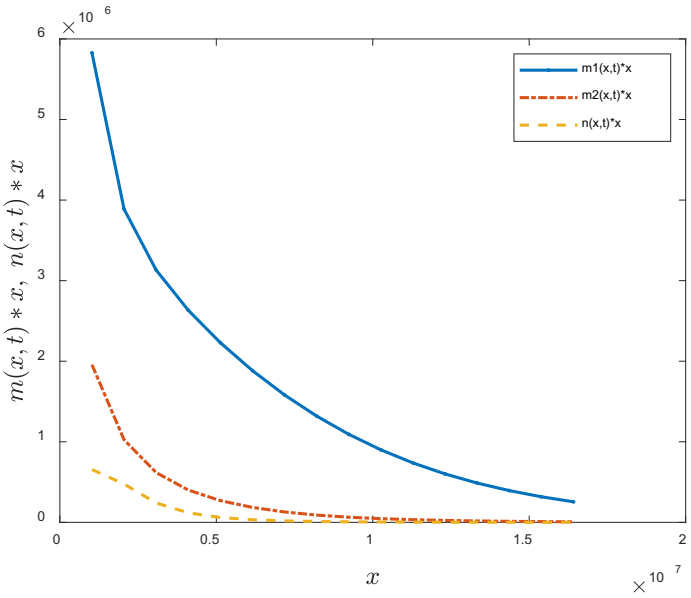

Fig. 6. Final cluster size weight distributions in the reference semicontinuous seeded emulsion polymerization. t = 13000 s. T = 80 °C. m1(x,t) and m2(x,t) refer to non-equilibrium clusters of size × at time t in the outer and inner regions, respectively, and n(x,t) to equilibrium clusters.

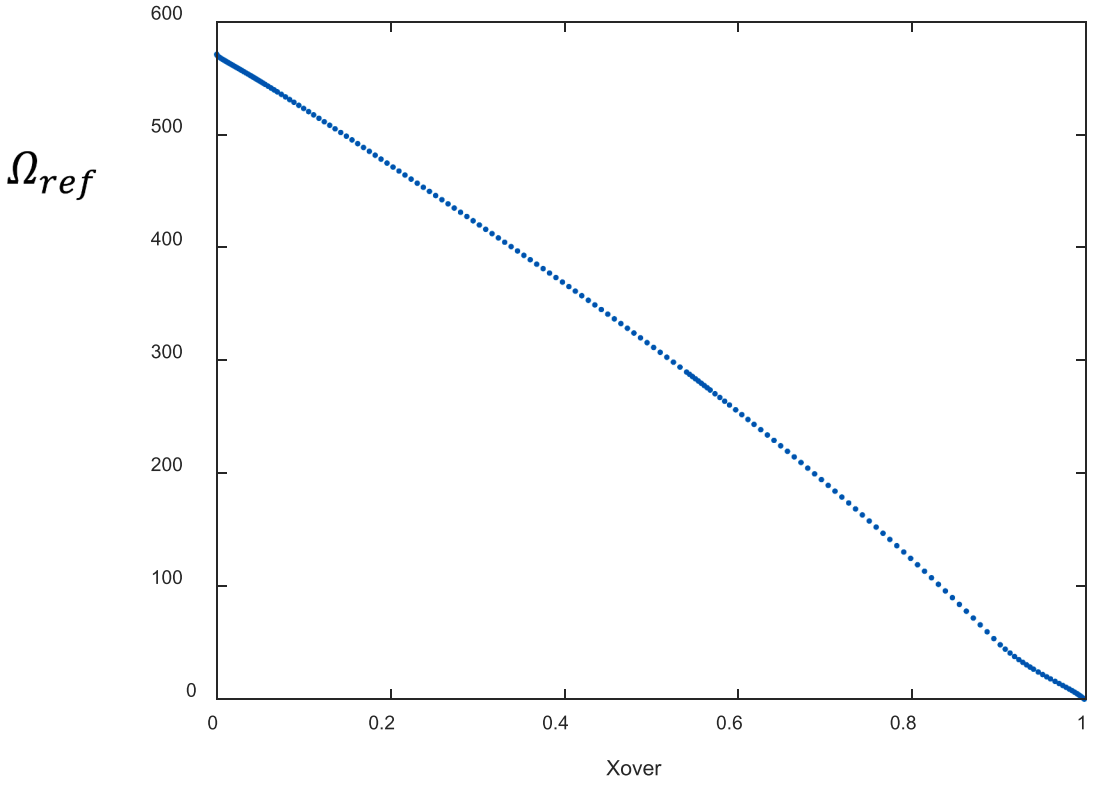

Fig. 7. Master trajectory derived from the reference experiment using Eq. (12).

translate directly to the distribution of particle morphologies present in the system and can be used to obtain representative particle morphologies by random sampling of the distribution as described in Ref [25]. It can be seen in Fig. 6 that most of the second stage polymer exists in small domains in the non-equilibrium position at the exterior of the particle (m1), thus the system represents a far-from-equilibrium morphology. The master curve calculated using Eqs. (11) and (12) from the evolution of the conversions, using the values of A, B and C in Table S1 is presented in Fig. 7.

If Fig. 7 is a master curve, any polymerization that fulfills this curve should give the same cluster size distribution presented in Fig. 6. First, the case in which the reaction temperature was that of the reference process (80 °C, constant during the process) and the instantaneous and overall conversions were varied was considered. This case represents a common practical situation where conversions are modified by changes in monomer and initiator feed rates, which are much easier to implement than changes in the temperature of a large reactor. In addition, modification of polymerization temperatures is problematic from a

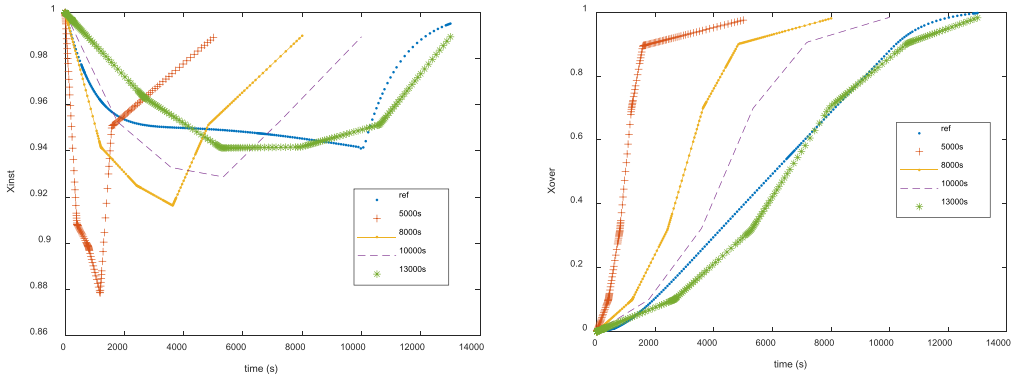

Fig. 8. Instantaneous and overall conversions of the four reaction trajectories calculated at 80 °C by means of Eq. (18). The conversions for the reference process are also included.

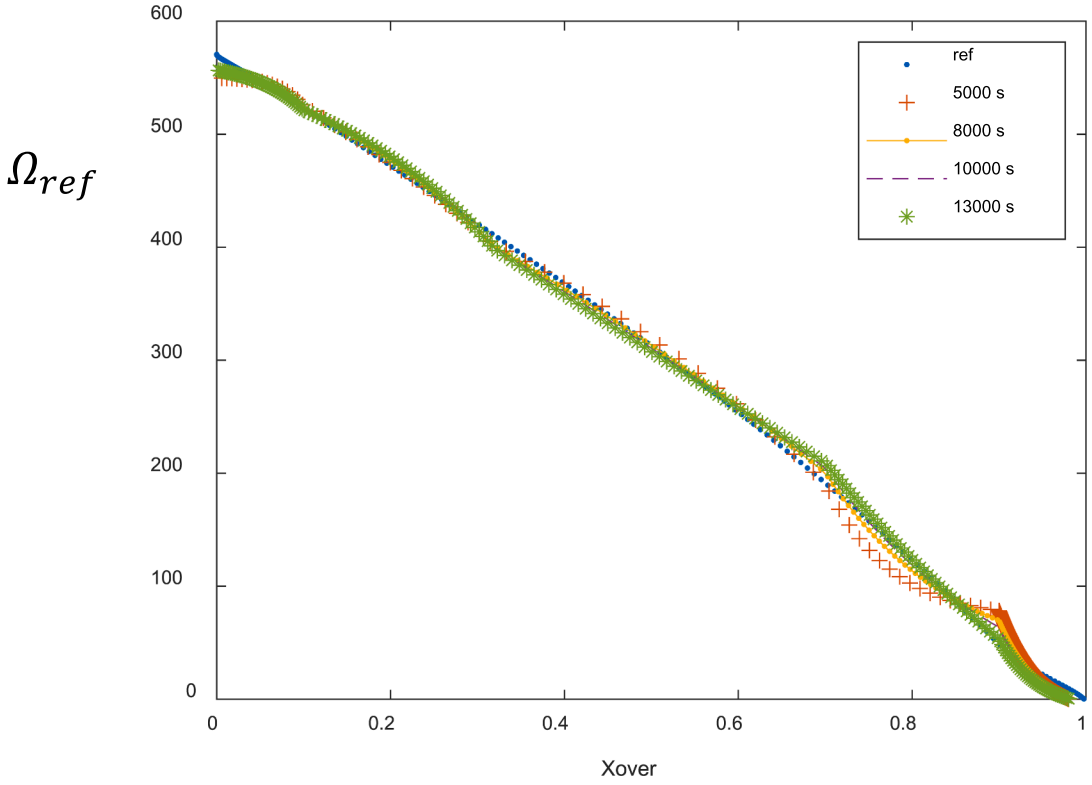

Fig. 9. Comparison between the cluster trajectories of the reference process and those of the processes in Fig. 8. T = 80 °C.

product point of view as it strongly affects polymer properties such as molecular weights.

For a known polymerization trajectory (evolution of overall and instantaneous conversion), the master curve of the process can be obtained by using the simple rheological model described in Eq. (13) to calculate the viscosity at a given reaction time and using the resulting viscosity-time relationship to calculate the master curve directly using Eq. (12). Different processes that fulfilled the master curve in Fig. 7 at 80 °C were calculated as

$$\min_{X_{inst}(t),X_{over}(t)} \int_0^{X_{overfinal}} \left(\Omega_{ref}\left(X_{over}, X_{overfinal}\right) - \Omega_{new}\left(X_{over}, X_{overfinal}\right)\right)^2 dX_{over} \tag{18}$$

This is a least squares regression in which the polymerization trajectory of a proposed new process is modified until the master curve of a proposed new process, Ω_{new}, matches that of the reference process, Ω_{ref}.

As discussed above, an almost infinite number of polymerization trajectories can yield the $\Omega\left(X_{over}, X_{overfinal}\right)$ shown in Fig. 7. Therefore, in order to restrict the number of alternatives, several constraints were imposed. The process was divided in five intervals of time. The first four intervals correspond to the semicontinuous operation (namely, $\sum_{i=1}^{4} t_i = t_{feed}$, where t_{feed} is the total feeding time) and the fifth interval was the final batch process. The four initial intervals had the same length ($t_{feed}/4$). The overall conversions at the end of the five intervals were fixed as $X_{over1} = 0.1$; $X_{over2} = 0.32$; $X_{over3} = 0.7$; $X_{overfeed} = 0.9$; and $X_{overfinal} = 0.98$. In addition, straight lines were used to describe the evolution of the overall and instantaneous conversions between these points. Furthermore, the material balances were fulfilled, namely the monomer (s) were completely fed by t_{feed}, and the monomer feeding rate was always greater or equal to zero. The latter constraint implies that monomer cannot be removed from the reactor. With these constraints, Eq. (18) was solved for estimating the values of the feeding period (t_{feed}) and

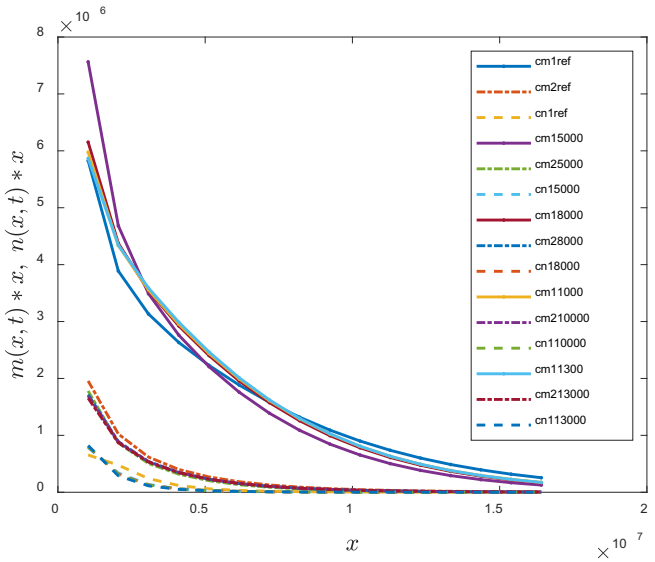

Fig. 10. Cluster size distributions obtained with the reaction trajectories in T = 80 °C. cm1 and cm2 refer to non-equilibrium clusters in the outer and inner regions, respectively, and cn to equilibrium clusters.

those of the X_{inst} at the end of the first four intervals. Notice that X_{inst} for the final time is determined by $X_{overfinal} = 0.98$. Eq. (18) was solved for the following final times: 5000 s, 8000 s, 10000 s and 13000 s. Although these values are chosen arbitrarily, they can be regarded as processes carried out in reactors with different heat removal capacity. The calculated reaction trajectories expressed in terms of the instantaneous and overall conversions are presented in Fig. 8. The instantaneous and overall conversions of the reference process are included for comparison. Fig. 9 shows that quite different processes yielded the same $\Omega(X_{over}, X_{overfinal})$. Therefore, if Fig. 7 is a master curve, these processes should give the same particle morphology.

The four processes were implemented in the mathematical model describing the process to calculate the particle morphology. To do so, the evolution of the instantaneous and overall conversions were used to calculate $\bar{n}N_p$, where $\bar{n}$ was the average number of radicals per particle, and N_p, the number of polymer particles. Fig. 10 presents a comparison of the cluster size distributions determined by the simulations for the four processes in Fig. 8 with those of the reference process. Note that as described in Ref [25] these cluster distributions can be directly related to the particle morphology as observed by TEM and therefore similar cluster size distributions indicate similar particle morphology distributions. As in the reference process, for the proposed new processes the primary location of the second stage polymer was in the non-equilibrium clusters at the outer region of the particle (bold lines in Fig. 10). Both the weight fraction and the domain size of clusters in this region was similar for all the proposed new processes, with a slightly higher fraction of small clusters in the case of the reaction conducted on the shortest timeframe (5000 s). Similarly, the amount and size of non-equilibrium clusters in the inner region of the particle and the equilibrium clusters were similar to the reference process in all cases. This similarity in the cluster size distribution and their location for processes conducted under significantly different reaction conditions demonstrates that $\Omega_{ref}(X_{over}, X_{overfinal})$ is a master curve. It is worth pointing out that the models used to calculate the morphology include cluster coalescence that is not specifically included in the master curve. This supports the assumption that coalescence is determined by cluster nucleation and migration. On the other hand, the constraints imposed on the shape of the evolutions for X_{inst} and X_{over} do not limit the generality of this conclusion.

In the previous discussion, the polymerization temperature was that of the reference process (80 °C, constant during the process). However,

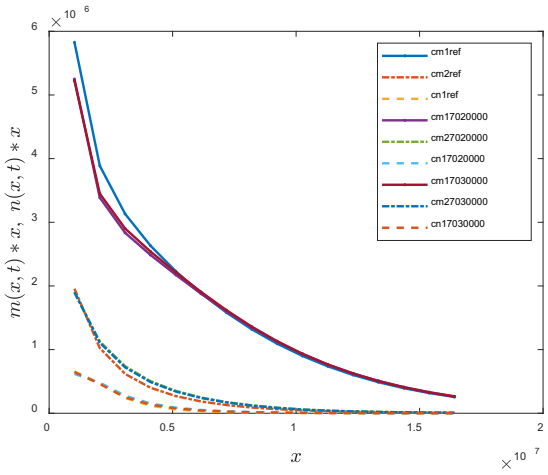

Fig. 11. Cluster size distributions obtained with the processes in Fig. S1. T = 70 °C.

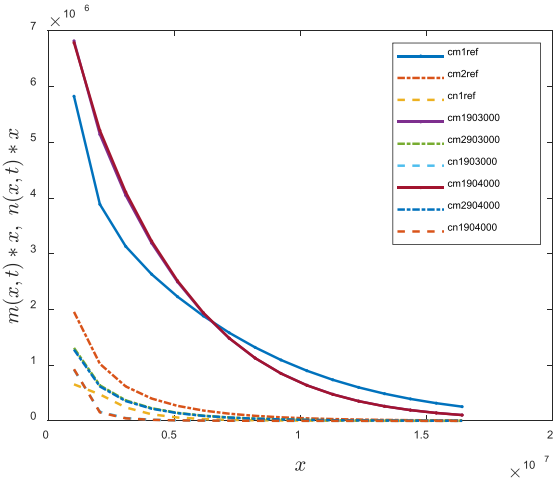

Fig. 12. Cluster size distributions obtained with the processes in Fig. S2. T = 90 °C.

although temperature is not often used as manipulated variable due to the time delays caused by the thermal inertia of large reactors and the effect of temperature on other polymer characteristics such as molecular weights, it is necessary to demonstrate that $\Omega_{ref}(X_{over}, X_{overfinal})$ in Fig. 7 is also a master curve when the polymerizations are carried out at temperatures different than that of the reference process. In order to do that, processes that fit the master curve in Fig. 7 were calculated as explained above for reactions conducted at 70 and 90 °C. This range of temperatures encompasses the temperatures most often used in emulsion polymerization. The final process times were adjusted to the reaction temperature. For 90 °C, as the heat removal rate increased, process times (3000 and 4000 s) shorter than for the reference process (that was carried out at 80 °C) were used. On the other hand, they were longer for 70 °C (20000 and 30000 s). The reaction trajectories are presented in Figs. S1 and S2 of the Supporting Information. These figures also include the comparison of the $\Omega(X_{over}, X_{overfinal})$ of these processes with that of the reference process. It can be seen that the calculated reaction trajectories gave $\Omega(X_{over}, X_{overfinal})$ close to that of the reference process. The calculated reaction trajectories were implemented in the model and used to obtain the predicted final cluster size distributions of the particles. Figs. 11 and 12 show that in all cases the cluster distributions were similar to the reference process which, as detailed above, indicates that

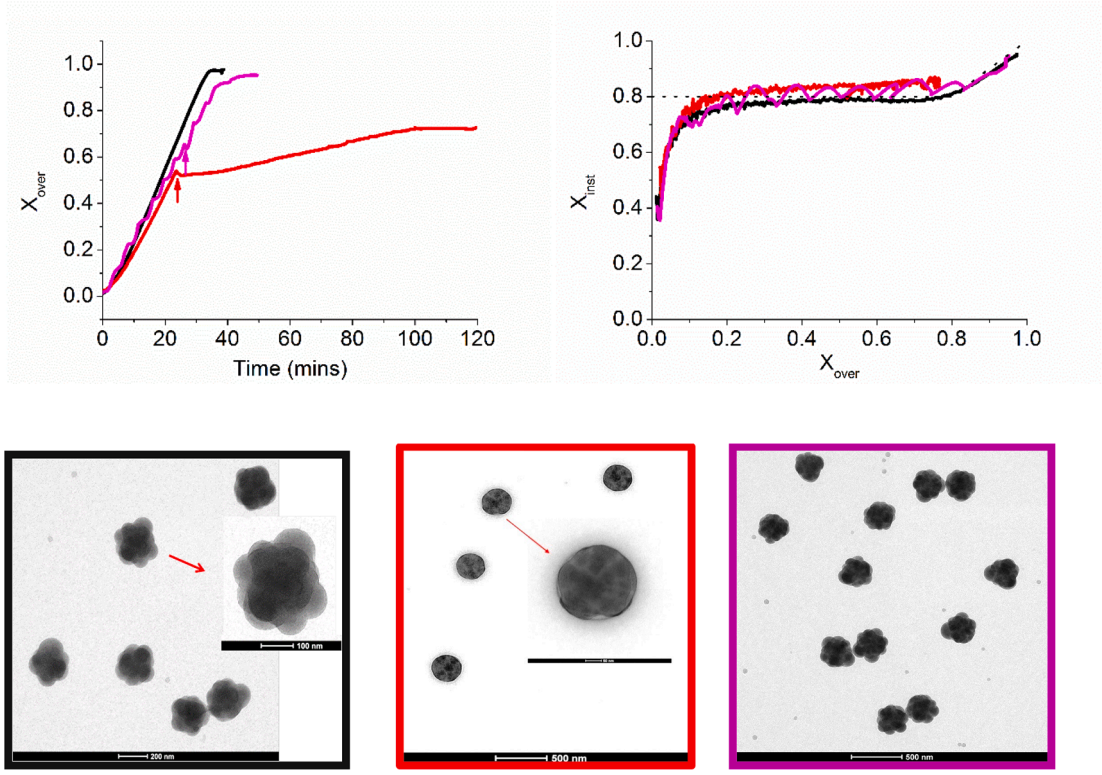

Fig. 13. (Top left) Evolution of overall conversion with time, (Top right) evolution of instantaneous conversion and (Bottom) TEM images for experimental results of Rajabalinia et al. [24]. Run 1 is the reference process (black, bottom left); Runs 2 (red, bottom center) and 3 (magenta, bottom right) are controlled processes where a shot of inhibitor was added (marked with arrows). In Run 2, the set point was the instantaneous conversion (dotted line in top right panel); and in Run 3, the evolutions of instantaneous and overall conversions were used as set points. T = 80 °C. Reprinted from [24], Copyright (2021), with permission from Elsevier.

they yielded particle morphologies that were very close to that of the reference process, offering further support that $\Omega_{ref}(X_{over}, X_{overfinal})$ is a master curve.

3.2. Experimental demonstration that $\Omega_{ref}(X_{over}, X_{overfinal})$ is a master trajectory

The previous section demonstrates *in silico* that $\Omega_{\mathrm{ref}}(\mathrm{X_{over}}, \mathrm{X_{overfinal}})$ is a master curve. In this section, we demonstrate that this conclusion is also supported by experimental data. For that, the system used by Rajabalinia et al. [24] was considered. The chemical system coincides with that used in the *in silico* demonstration. This was a seeded semi-continuous emulsion copolymerization of S and BA using an MMA/BA seed carried out at 80 °C.

In that work, Rajabalinia *et al.* controlled the particle morphology by means of a control strategy that used the evolutions of the instantaneous and overall conversions of the reference process as set point. This strategy successfully controlled the particle morphology in the presence of disturbances caused by a shot of inhibitor during the semicontinuous operation. When only the evolution of the instantaneous conversion was used as set point, control of particle morphology was not possible. Fig. 13 presents the evolutions of the overall and instantaneous conversions in these experiments as well as images of the particles obtained. In this figure, Run 1 is the reference process; Run 2 the process in which the set point was the instantaneous conversion and a shot of inhibitor was added (marked with an arrow); and Run 3 is the controlled process using the evolutions of both instantaneous and overall conversions as set points (the shot of inhibitor was marked with an arrow). The feeding profiles of monomer and reductant for these reactions are shown in Fig. S3 of the supporting information using the experiments conducted in Ref. [24].

The $\Omega(X_{over}, X_{overfinal})$ of these reactions were calculated using the

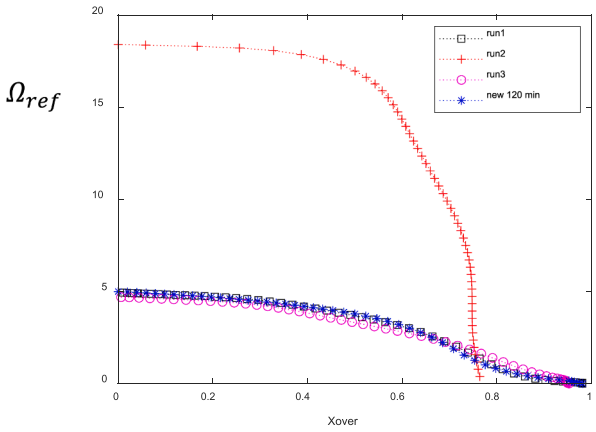

Fig. 14. $\Omega(X_{over}, X_{overfinal})$ for Runs 1–3 in ref [24] as well as for the newly designed experiment.

evolutions of the instantaneous and overall conversions and the same rheological model as in the *in silico* demonstration (Fig. 14). Admittedly, this model may not be completely accurate for the experiments and there are a number of potential sources of error, most of which are common for rheological models of concentrated polymer solutions. First, the estimate of the effective T_g (Eq. (14)) is dependent on the values of the glass transition temperatures of the monomers, which are unknowns and are estimated from the melting points of the monomers. Furthermore, although common estimates of the parameter K and the 5th power dependence of polymer volume fraction are used, if these values are not accurate, deviations may be expected when using the

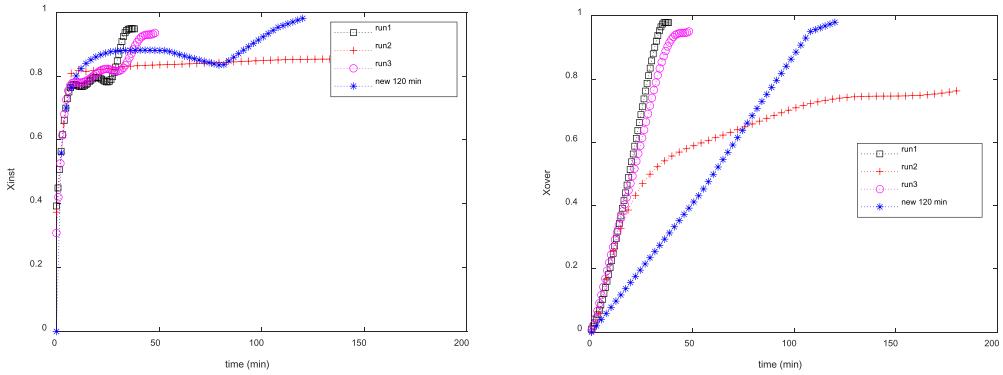

Fig. 15. Comparison of the calculated evolutions of the instantaneous and overall conversion of the new process with those of Runs 1–3.

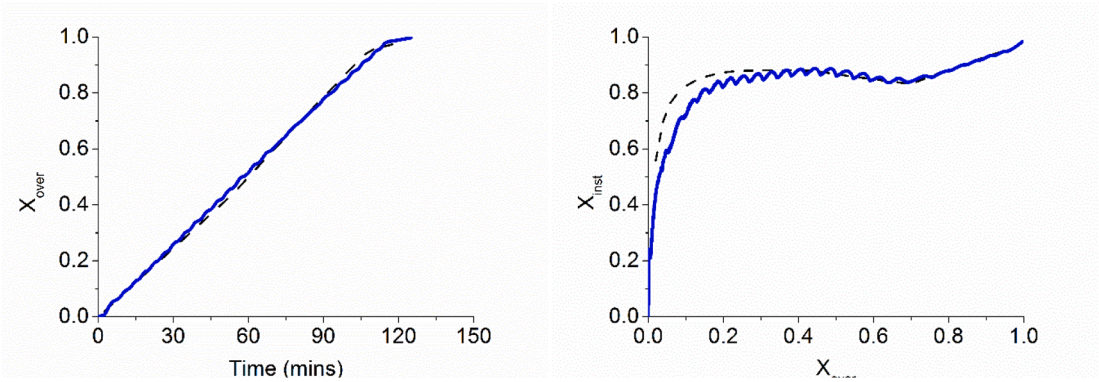

Fig. 16. (Left) Evolution of overall conversion with time and (right) evolution of instantaneous conversion. The blue lines show the experimentally obtained values and the black dashed line show the target values as determined from the master trajectories.

master curve to design processes conducted at different instantaneous conversions (different polymer volume fractions) and reaction temperatures (different $T_{geffect}/T$). The other empirical constants in Eq. (13) are also potential sources of error but in the present case they should be close enough as these constants have been used to fit the effect of the process conditions on particle morphology for this system [26]. Fig. 14 shows that $\Omega(X_{over}, X_{overfinal})$ of Runs 1 and 3 were very close and that that of Run 2 was above. These results are consistent with the particle morphologies in Fig. 13 that show that the cluster penetrated more in Run 2 (higher value of $\Omega(X_{over}, X_{overfinal})$).

As Run 1 was the reference experiment its $\Omega(X_{over}, X_{overfinal})$ was considered to be the master curve and it was used to determine the polymerization trajectory of another reaction with a final time of 120 min using Eq. (18). Fig. 15 compares the desired evolution of the instantaneous and overall conversion of the new experiment with those of Runs 1–3. It can be seen that the new experiment is clearly different from the previous experiments. Nevertheless, in spite of these differences it presents the same $\Omega(X_{over}, X_{overfinal})$ as Runs 1 and 3 (Fig. 14).

A seeded semicontinuous emulsion polymerization aimed at following the trajectories of the new experiment was carried out (Run 4). For that, the on-line control of the evolutions of the instantaneous and overall conversions was implemented in a calorimeter reactor using the calculated trajectories as set point and following the procedure described in reference [24]. The feeding profile for the monomer and reductant in these experiments is shown in Fig. S3 in the supporting information. Fig. 16 shows that the on-line control was successful and that the experimental evolutions of X_{inst} and X_{over} closely tracked the set point. At low overall conversion there are some differences between the target and the experimental values of X_{inst} due to challenges associated with the initial control of the process but this is resolved at relatively short times/low conversions.

TEM images of the particle morphology were obtained following the method described in reference [26] (Fig. 17). For comparison, images at a similar scale are shown for Run 3 in which the process conditions were drastically different but has similar $\Omega(X_{over}, X_{overfinal})$. The particle morphology was very close in both cases, further demonstrating that $\Omega(X_{over}, X_{overfinal})$ is a master curve.

4. Perspectives and opportunities

The existence of the master curves opens a completely new scenario for both on-line control of the morphology of waterborne dispersed particles and process optimization. First, as demonstrated above, it makes it possible to efficiently control particle morphology on-line by following a trajectory that is defined by the instantaneous and overall monomer conversions and the reactor temperature, which are variables that can be easily monitored in real time.

In addition, the master curve can be used as a constraint in process optimization. For example, if the process is transferred to another facility where the cooling system is more efficient, the polymerization can be carried out in a shorter time, but a proportional increase of the feeding rates will lead to a different morphology. With the master curve, following the method outlined above, a new polymerization trajectory can be found that yields the same morphology but with shorter reaction times. Similarly, if the process is transferred to a reactor with lower heat removal capacity per unit volume (for example, because a larger reactor is used) an alternative reaction trajectory leading to the same particle morphology can be obtained.

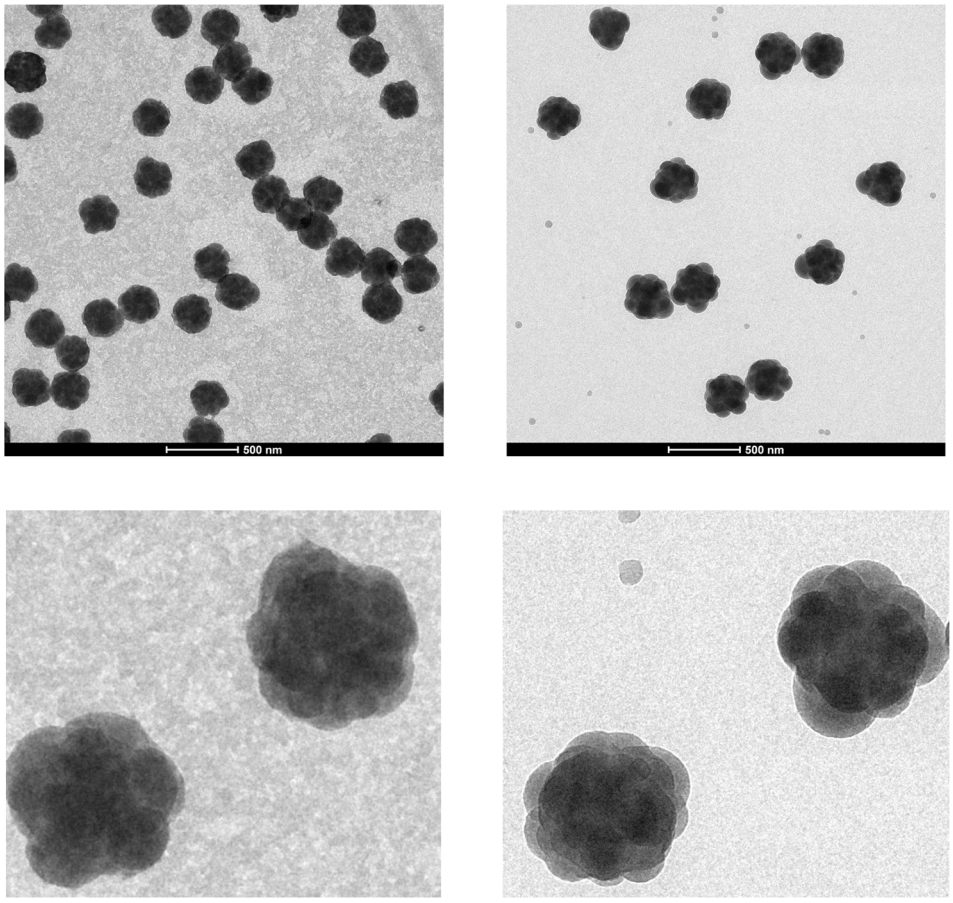

Fig. 17. TEM images showing the new process with extended reaction times (Run 4, left) and a process that follows exactly the conditions of the reference process (Run 3, right).

5. Conclusions

This article addresses the long-standing and so far unsolved problem of the on-line control of particle morphology. We have shown that the development of particle morphology can be understood in terms of the phase separation and migration processes, leading to a "master trajectory" that defines the final particle morphology. Using these master curves the polymerization process can be designed to give a particle morphology that matches that of a reference process but with different overall reaction times and/or reaction temperatures. The validity of this concept has been demonstrated by using both *in silico* and experimental data. As the master curves can be determined during the process from available online measurements (monomer conversions and reactor temperature), this opens the way for the online control of the particle morphology. In addition, the use of master curves facilitates process optimization when the process should be transferred to reactors with different cooling capacity.

Declaration of Competing Interest

The authors declare that they have no known competing financial interests or personal relationships that could have appeared to influence the work reported in this paper.

Appendix A. Supplementary data

Supplementary data to this article can be found online at https://doi.org/10.1016/j.cej.2021.131508.

References

[1] R. Udagama, C. de las Heras Alarcón, J.L. Keddie, J.G. Tsavalas, E. Bourgeat-Lami, T.F.L. McKenna, Acrylic-Alkyd Hybrids: Secondary Nucleation, Particle Morphology, and Limiting Conversions, Macromol. React. Eng. 8 (9) (2014) 622–638, https://doi.org/10.1002/mren.201400003.
[2] B. Schuler, R. Baumstark, S. Kirsch, A. Pfau, M. Sandor, A. Zosel, Structure and properties of multiphase particles and their impact on the performance of architectural coatings, Prog. Org. Coatings. 40 (1-4) (2000) 139–150, https://doi.org/10.1016/S0300-9440(00)00136-3.
[3] F. Domingues Dos Santos, P. Fabre, X. Drujon, G. Meunier, L. Leibler, Films from soft-core/hard-shell hydrophobic latexes: Structure and thermomechanical properties, J. Polym. Sci. Part B Polym. Phys. 38 (2000) 2989–3000, https://doi.org/10.1002/1099-0488(20001201)38:23<2989::AID-POLB10>3.0.CO;2-D.
[4] J. Geurts, J. Bouman, A. Overbeek, New waterborne acrylic binders for zero VOC paints, J. Coatings Technol. Res. 5 (1) (2008) 57–63, https://doi.org/10.1007/s11998-007-9036-x.
[5] E. Limousin, N. Ballard, J.M. Asua, The influence of particle morphology on the structure and mechanical properties of films cast from hybrid latexes, Prog. Org. Coatings. 129 (2019) 69–76, https://doi.org/10.1016/j.porgcoat.2019.01.015.
[6] E. Limousin, N. Ballard, J.M. Asua, Soft core–hard shell latex particles for mechanically strong VOC-free polymer films, J. Appl. Polym. Sci. 136 (23) (2019) 47608, https://doi.org/10.1002/app.v136.2310.1002/app.47608.
[7] E. Degrandi-Contraires, R. Udagama, E. Bourgeat-Lami, T. McKenna, K. Ouzineb, C. Creton, Mechanical Properties of Adhesive Films Obtained from PU/Acrylic Hybrid Particles, Macromolecules. 44 (2011) 2643–2652.
[8] R. Udagama, E. Degrandi-Contraires, C. Creton, C. Graillat, T.F.L. McKenna, E. Bourgeat-Lami, Synthesis of AcrylicÀPolyurethane Hybrid Latexes by Miniemulsion Polymerization and Their Pressure-Sensitive Adhesive Applications, Macromolecules. 44 (2011) 2632–2642.
[9] A. Lopez, Y. Reyes, E. Degrandi-Contraires, E. Canetta, C. Creton, J.M. Asua, Waterborne hybrid polymer particles: Tuning of the adhesive performance by controlling the hybrid microstructure, Eur. Polym. J. 49 (6) (2013) 1541–1552, https://doi.org/10.1016/j.eurpolymj.2013.01.030.
[10] A.B. Foster, P.A. Lovell, M.A. Rabjohns, Control of adhesive properties through structured particle design of water-borne pressure-sensitive adhesives, Polymer. 50 (7) (2009) 1654–1670, https://doi.org/10.1016/j.polymer.2009.01.054.

[11] T.Y. Guo, G.L. Tang, G.J. Hao, M.D. Song, B.H. Zhang, Toughening modification of PS with n-BA/MMA/styrene core-shell structured copolymer from emulsifier-free emulsion polymerization, J. Appl. Polym. Sci. 90 (5) (2003) 1290–1297, https://doi.org/10.1002/(ISSN)1097-462810.1002/app.v90:510.1002/app.12752.
[12] S. Caimi, E. Timmerer, M. Banfi, G. Storti, M. Morbidelli, Core-Shell Morphology of Redispersible Powders in Polymer-Cement Waterproof Mortars, Polymers (Basel). 10 (10) (2018) 1122, https://doi.org/10.3390/polym10101122.
[13] C.-L. Lin, W.-Y. Chiu, C.-F. Lee, Thermal/pH-sensitive core-shell copolymer latex and its potential for targeting drug carrier application, Polymer. 46 (2005) 10092–10101, https://doi.org/10.1016/j.polymer.2005.07.098.
[14] S. Torza, S.G. Mason, Three-phase interactions in shear and electrical fields, J. Colloid Interface Sci. 33 (1970) 67–83, https://doi.org/10.1016/0021-9797(70)90073-1.
[15] Y.G. Durant, D.C. Sundberg, An advanced computer algorithm for determining morphology development in latex particles, J. Appl. Polym. Sci. 58 (1995) 1607–1618, https://doi.org/10.1002/app.1995.070580924.
[16] D.C. Sundberg, Y.G. Durant, Latex Particle Morphology, Fundamental Aspects: A Review, Polym. React. Eng. 11 (3) (2003) 379–432, https://doi.org/10.1081/PRE-120024420.
[17] O.J. Karlsson, J.M. Stubbs, R.H. Carrier, D.C. Sundberg, Dynamic Modeling of Non-equilibrium Latex Particle Morphology Development During Seeded Emulsion Polymerization, Polym. React. Eng. 11 (4) (2003) 589–625, https://doi.org/10.1081/PRE-120026365.
[18] J.M. Stubb, D.C. Sundberg, Nonequilibrium Morphology Development in Seeded Emulsion Polymerization. IV. Influence of Chain Transfer Agent, J. Appl. Polym. Sci. 102 (2) (2006) 945–957, https://doi.org/10.1002/(ISSN)1097-462810.1002/app.v102:210.1002/app.23643.
[19] L.J. Gonzalez-Ortiz, J.M. Asua, Development of Particle Morphology in Emulsion Polymerization. 1. Cluster Dynamics, Macromolecules. 28 (9) (1995) 3135–3145, https://doi.org/10.1021/ma00113a016.
[20] J.M. Stubbs, D.C. Sundberg, The dynamics of morphology development in multiphase latex particles, Prog. Org. Coatings. 61 (2-4) (2008) 156–165, https://doi.org/10.1016/j.porgcoat.2007.09.038.
[21] S. Jiang, A. Van Dyk, A. Maurice, J. Bohling, D. Fasano, S. Brownell, Design colloidal particle morphology and self-assembly for coating applications, Chem. Soc. Rev. 46 (12) (2017) 3792–3807, https://doi.org/10.1039/C6CS00807K.
[22] W. Gerlinger, J.M. Asua, T. Chaloupka, J.M.M. Faust, F. Gjertsen, S. Hamzehlou, S. O. Hauger, E. Jahns, P.J. Joy, J. Kosek, A. Lapkin, J.R. Leiza, A. Mhamdi, A. Mitsos, O. Naeem, N. Rajabalinia, P. Singstad, J. Suberu, Dynamic Optimization and Non-linear Model Predictive Control to Achieve Targeted Particle Morphologies, Chemie-Ingenieur-Technik. 91 (2019) 323–335, https://doi.org/10.1002/cite.201800118.
[23] J.M. Asua, Emulsion polymerization: From fundamental mechanisms to process developments, J. Polym. Sci. Part A Polym. Chem. 42 (5) (2004) 1025–1041, https://doi.org/10.1002/pola.11096.
[24] N. Rajabalinia, N. Ballard, S. Hamzehlou, J.R. Leiza, J.M. Asua, On-line control of the particle morphology of composite polymer-polymer waterborne dispersions, Chem. Eng. J. 408 (2021) 127253, https://doi.org/10.1016/j.cej.2020.127253.
[25] S. Hamzehlou, J.R. Leiza, J.M. Asua, A new approach for mathematical modeling of the dynamic development of particle morphology, Chem. Eng. J. 304 (2016) 655–666, https://doi.org/10.1016/j.cej.2016.06.127.
[26] N. Rajabalinia, S. Hamzehlou, J.R.J.R. Leiza, J.M.J.M. Asua, Experimental validation of a mathematical model for the evolution of the particle morphology of waterborne polymer-polymer hybrids: Paving the way to the design and implementation of optimal polymerization strategies, Chem. Eng. J. 363 (2019) 259–269.
[27] S. Hamzehlou, M. Aguirre, J.R. Leiza, J.M. Asua, Dynamics of the Particle Morphology during the Synthesis of Waterborne Polymer-Inorganic Hybrids, Macromolecules. 50 (18) (2017) 7190–7201, https://doi.org/10.1021/acs.macromol.7b0148810.1021/acs.macromol.7b01488.s001.
[28] J.M.M. Faust, S. Hamzehlou, J.R. Leiza, J.M. Asua, A. Mhamdi, A. Mitsos, Dynamic optimization of a two-stage emulsion polymerization to obtain desired particle morphologies, Chem. Eng. J. 359 (2019) 1035–1045, https://doi.org/10.1016/J.CEJ.2018.11.081.
[29] J.M.M. Faust, S. Hamzehlou, J.R. Leiza, J.M. Asua, A. Mhamdi, A. Mitsos, Closed-loop in-silico control of a two-stage emulsion polymerization to obtain desired particle morphologies, Chem. Eng. J. 414 (2021), 128808, https://doi.org/10.1016/j.cej.2021.128808.
[30] D.C. Sundberg, A.P. Casassa, J. Pantazopoulos, M.R. Muscato, B. Kronberg, J. Berg, Morphology development of polymeric microparticles in aqueous dispersions. I. Thermodynamic considerations, J. Appl. Polym. Sci. 41 (1990) 1425–1442, https://doi.org/10.1002/app.1990.070410706.
[31] Y.-C. Chen, V. Dimonie, M.S. El-Aasser, Interfacial phenomena controlling particle morphology of composite latexes, J. Appl. Polym. Sci. 42 (1991) 1049–1063, https://doi.org/10.1002/app.1991.070420418.
[32] D.W. van Krevelen, K. te Nijenhuis, Properties of Polymers 4th Edition: Their Correlation with Chemical Structure; their Numerical Estimation and Prediction from Additive Group Contributions, Elsevier Science, 2009.
[33] F. Bueche, Rate and Pressure Effects in Polymers and Other Glass-Forming Substances, J. Chem. Phys. 36 (11) (1962) 2940–2946, https://doi.org/10.1063/1.1732405.
[34] P.D. Armitage, J.C. De La Cal, J.M. Asua, Improved methods for solving monomer partitioning in emulsion copolymer systems, J. Appl. Polym. Sci. 51 (1994) 1985–1990, https://doi.org/10.1002/app.1994.070511201.
[35] L.M. Gugliotta, G. Arzamendi, J.M. Asua, Choice of monomer partition model in mathematical modeling of emulsion copolymerization systems, J. Appl. Polym. Sci. 55 (1995) 1017–1039, https://doi.org/10.1002/app.1995.070550706.